



THE UNIVERSITY *of* EDINBURGH

Edinburgh Research Explorer

3D spatial exploration by E. coli echoes motor temporal variability

Citation for published version:

Figueroa-Morales, N, Soto, R, Junot, G, Darnige, T, Douarche, C, Martinez, V, Lindner, A & Clément, E 2020, '3D spatial exploration by E. coli echoes motor temporal variability', *Physical Review X*, vol. 10, no. 2, 021004. <https://doi.org/10.1103/PhysRevX.10.021004>

Digital Object Identifier (DOI):

[10.1103/PhysRevX.10.021004](https://doi.org/10.1103/PhysRevX.10.021004)

Link:

[Link to publication record in Edinburgh Research Explorer](#)

Document Version:

Peer reviewed version

Published In:

Physical Review X

General rights

Copyright for the publications made accessible via the Edinburgh Research Explorer is retained by the author(s) and / or other copyright owners and it is a condition of accessing these publications that users recognise and abide by the legal requirements associated with these rights.

Take down policy

The University of Edinburgh has made every reasonable effort to ensure that Edinburgh Research Explorer content complies with UK legislation. If you believe that the public display of this file breaches copyright please contact openaccess@ed.ac.uk providing details, and we will remove access to the work immediately and investigate your claim.



Important Notice to Authors

No further publication processing will occur until we receive your response to this proof.

Attached is a PDF proof of your forthcoming article in *Physical Review X*. The article accession code is XU10353.

Your paper has been assigned the following Subject Area labels: Biological Physics, Interdisciplinary Physics, Soft Matter
Your paper will be in the following section of the journal: RESEARCH ARTICLES

Please note that as part of the production process, APS converts all articles, regardless of their original source, into standardized XML that in turn is used to create the PDF and online versions of the article as well as to populate third-party systems such as Portico, Crossref, and Web of Science. We share our authors' high expectations for the fidelity of the conversion into XML and for the accuracy and appearance of the final, formatted PDF. This process works exceptionally well for the vast majority of articles; however, please check carefully all key elements of your PDF proof, particularly any equations or tables.


Figures submitted electronically as separate files containing color appear in color in the journal.

Specific Questions and Comments to Address for This Paper

The numbered items below correspond to numbers in the margin of the proof pages pinpointing the source of the question and/or comment. The numbers will be removed from the margins prior to publication.

- 1 Third proof:** Please note that only funding organization names are allowed in “Funding Information” section, program number has been fixed as per PRX style.
- 2 Third proof:** Please check very closely to confirm all of the corrections have been incorporated properly throughout this Letter and also approve **the Letter is ready to be published in its current form.**

ORCIDs

Please follow any ORCID links () after the authors' names and verify that they point to the appropriate record for each author.

Funding Information

Information about an article's funding sources is now submitted to Crossref to help you comply with current or future funding agency mandates. Crossref's Open Funder Registry (<https://www.crossref.org/services/funder-registry/>) is the definitive registry of funding agencies. Please ensure that your acknowledgments include all sources of funding for your article following any requirements of your funding sources. Where possible, please include grant and award ids. Please carefully check the following funder information we have already extracted from your article and ensure its accuracy and completeness:

- Agence Nationale de la Recherche, FundRef ID <http://dx.doi.org/10.13039/501100001665> (FR/Republic of France)
- Franco-Chilean Ecosud Collaborative Program
- Pierre-Gilles de Gennes Foundation
- H2020 European Research Council, FundRef ID <http://dx.doi.org/10.13039/100010663> (EU/European Union)
- Fondo Nacional de Desarrollo Científico y Tecnológico, FundRef ID <http://dx.doi.org/10.13039/501100002850> (CL/ Republic of Chile)
- Ministerio de Economía, Fomento y Turismo, FundRef ID <http://dx.doi.org/10.13039/501100005886> (CL/Republic of Chile)

- H2020 European Research Council, FundRef ID <http://dx.doi.org/10.13039/100010663> (EU/European Union)
- École Supérieure de Physique et de Chimie Industrielles de la Ville de Paris, FundRef ID <http://dx.doi.org/10.13039/501100003068> (FR/Republic of France)
- Laboratoire International Associé “Matière: Structure et dynamique” (LIA-MSD)
- Centre National de la Recherche Scientifique, FundRef ID <http://dx.doi.org/10.13039/501100004794> (FR/Republic of France)
- Institut Pierre-Gilles de Gennes (Équipement d'Excellence, “Investissements d'avenir”)

Other Items to Check

- Please note that the original manuscript has been converted to XML prior to the creation of the PDF proof, as described above. Please carefully check all key elements of the paper, particularly the equations and tabular data.
- Please ignore the text of the Popular Summary, it is not the final version. An APS science writer will work with you separately to edit the summary.
- Title: Please check; be mindful that the title may have been changed during the peer-review process.
- Author list: Please make sure all authors are presented, in the appropriate order, and that all names are spelled correctly.
- Please make sure you have inserted a byline footnote containing the email address for the corresponding author, if desired. Please note that this is not inserted automatically by this journal.
- Affiliations: Please check to be sure the institution names are spelled correctly and attributed to the appropriate author(s).
- Receipt date: Please confirm accuracy.
- Acknowledgments: Please be sure to appropriately acknowledge all funding sources.
- Hyphenation: Please note hyphens may have been inserted in word pairs that function as adjectives when they occur before a noun, as in “x-ray diffraction,” “4-mm-long gas cell,” and “*R*-matrix theory.” However, hyphens are deleted from word pairs when they are not used as adjectives before nouns, as in “emission by x rays,” “was 4 mm in length,” and “the *R* matrix is tested.”
Note also that Physical Review follows U.S. English guidelines in that hyphens are not used after prefixes or before suffixes: superresolution, quasiequilibrium, nanoprecipitates, resonancelike, clockwise.
- Please check that your figures are accurate and sized properly. Make sure all labeling is sufficiently legible. Figure quality in this proof is representative of the quality to be used in the online journal. To achieve manageable file size for online delivery, some compression and downsampling of figures may have occurred. Fine details may have become somewhat fuzzy, especially in color figures. Figures to be published in color online will appear in color on these proofs if viewed on a color monitor or printed on a color printer.
- Overall, please proofread the entire *formatted* article very carefully. The redlined PDF should be used as a guide to see changes that were made during copyediting. However, note that some changes to math and/or layout may not be indicated.

Ways to Respond

- **Web:** If you accessed this proof online, follow the instructions on the web page to submit corrections.
- **Email:** Send corrections to aps-robot@luminad.com. Include the accession code XU10353 in the subject line.
- **Fax:** Return this proof with corrections to +1.855.808.3897.

If You Need to Call Us

You may leave a voicemail message at +1.855.808.3897. Please reference the accession code and the first author of your article in your voicemail message. We will respond to you via email.

Popular Summary

Bacterial motion determines the changing structure of microbial communities and controls infection spreading as well as microbiota organization in ecosystems. *E. coli* bacteria explore their environment using a “run-and-tumble” strategy: a sequence of straight paths (runs) and sudden changes in swimming direction (tumbles) that happen when motors driving the cell’s tail-like flagellum change rotation direction for a short time. While this random walk is classically described as a process with a single characteristic run time, the flagellar motor rotation switching, responsible for reorientations, displays a wide distribution of times. To address this paradox, we built a 3D tracking microscope suited to follow swimming bacteria for as long as tens of minutes.

Our results reconcile individual motor rotation and bacterial spatial exploration in three dimensions. We reveal a continuous variation of exploration “moods” for individual bacteria, characterized by periods of frequent directional changes alternating with periods of persistent swimming. The dynamics can be explained by important fluctuations in the number of certain proteins inside the cell that are responsible for the motor switching.

Future research will address the importance of these realistic run-and-tumble statistics in the macroscopic transport of bacteria. Bacterial persistent swimming may help to explain the onset of medical emergencies as well as bacterial anomalous transport in confined environments, such as narrow capillaries and porous media. This knowledge could be relevant to emerging technologies for targeted drug delivery or for understanding the spreading of biocontaminants in soils.

3D Spatial Exploration by *E. coli* Echoes Motor Temporal Variability

Nuris Figueroa-Morales^{1,2}, Rodrigo Soto³, Gaspard Junot¹, Thierry Darnige¹, Carine Douarache⁴,
Vincent A. Martinez⁵, Anke Lindner¹ and Éric Clément^{1,*}

¹*PMMH, UMR 7636 CNRS, ESPCI-Paris, PSL Research University, Sorbonne Université, Université de Paris, 7-9 quai Saint-Bernard, 75005 Paris, France*

²*Department of Biomedical Engineering, The Pennsylvania State University, University Park, Pennsylvania 16802, USA*

³*Departamento de Física, FCFM, Universidad de Chile, Santiago 8370448, Chile*

⁴*Université Paris-Saclay, CNRS, FAST, 91405 Orsay, France*

⁵*SUPA and School of Physics & Astronomy, The University of Edinburgh, Edinburgh EH9 3FD, United Kingdom*

(Received 6 January 2020; accepted 26 February 2020)

Unraveling bacterial strategies for spatial exploration is crucial for understanding the complexity in the organization of life. Bacterial motility determines the spatiotemporal structure of microbial and controls infection spreading and the microbiota organization in guts or in soils. Most theoretical approaches for modeling bacterial transport rely on their run-and-tumble motion. For *Escherichia coli*, the run-time distribution is reported to follow a Poisson process with a single characteristic time related to the rotational switching of the flagellar motors. However, direct measurements on flagellar motors show heavy-tailed distributions of rotation times stemming from the intrinsic noise in the chemotactic mechanism. Currently, there is no direct experimental evidence that the stochasticity in the chemotactic machinery affects the macroscopic motility of bacteria. In stark contrast with the accepted vision of run and tumble, here we report a large behavioral variability of wild-type *E. coli*, revealed in their three-dimensional trajectories. At short observation times, a large distribution of run times is measured on a population and attributed to the slow fluctuations of a signaling protein triggering the flagellar motor reversal. Over long times, individual bacteria undergo significant changes in motility. We demonstrate that such a large distribution of run times introduces measurement biases in most practical situations. Our results reconcile the notorious conundrum between run-time observations and motor-switching statistics. We finally propose that statistical modeling of transport properties, currently undertaken in the emerging framework of active matter studies, should be reconsidered under the scope of this large variability of motility features.

DOI:

Subject Areas: Biological Physics,
Interdisciplinary Physics, Soft Matter

I. INTRODUCTION

The *run-and-tumble* (R&T) strategy developed by bacteria for exploring their environment is a cornerstone of quantitative modeling of bacterial transport. In this paradigm, bacteria swim straight during a *run time*, undergo a reorientation process during a *tumbling time*, and pursue thereafter the next run in a different direction. The now standard vision of the R&T strategy was established in the 1970s for swimming *Escherichia coli* by Berg and Brown [1,2], based on 3D trajectories obtained via a Lagrangian

tracking technique. They proposed that an adapted bacterium would perform, over long times, an isotropic random walk composed of the run-and-tumble phases, both distributed in time as a Poisson process [1–5]. For quantitative analysis, the run-time and tumble-time distributions are often taken as Poisson processes with typical values $\bar{\tau}_{\text{run}} \sim 1$ s and $\bar{\tau}_{\text{tumble}} \sim 1/10$ s [2,6]. These values change in the presence of chemical gradients, leading to a biased random walk known as chemotaxis.

Alongside the relevance of this result in the context of biology, medicine, or ecology, fluids laden with motile bacteria have become an epitome for active matter, where the organization of active particles recently led scientists to revisit many concepts of out-of-equilibrium statistical physics [7–10]. Suspensions of motile bacteria are systems of choice for these studies [11], and many original phenomena such as anti-Fick’s law migration [12], collective motion [13], viscosity reduction [14–16], enhanced

*eric.clement@upmc.fr

Published by the American Physical Society under the terms of the Creative Commons Attribution 4.0 International license. Further distribution of this work must maintain attribution to the author(s) and the published article’s title, journal citation, and DOI.

diffusion [7], or motion rectification [17–20] have been discovered. Most recent theoretical studies on active matter, aimed at understanding the emergence of collective motion or other macroscopic transport processes in bacterial fluids, assume uncorrelated orientational noise, which is the direct consequence of the Poisson character of the R&T process [9].

The simple approach of introducing a Poisson distribution for the run times, although useful for simple qualitative interpretations, is not fully consistent with a growing number of measurements performed on the individual rotary motors [21–25] driving the helix-shaped flagella. For *E. coli*, the forward (run) motion is associated with the counterclockwise (CCW) rotation of the motors, and the tumbles take place when the motors rotate clockwise (CW). The CCW to CW transition is regulated by an internal biochemical process associated with the phosphorylation of the CheY protein.

In a seminal work, Korobkova *et al.* [21] brought evidence for a heavy tail distribution for the duration of CCW rotations. Importantly, this highlights possible coupling between the stochastic fluctuations in the chemotactic biochemical network and the emergent bacterial motility. Its consequences could affect the macroscopic organization of bacterial populations, chemotactic response to chemical heterogeneity, and genetic and epigenetic feedback of bacterial populations to environmental constraints.

Its potential importance in the context of active matter studies remains overlooked. For multiflagellated bacteria, the correspondence between switching statistics, motor synchronization, flagellar bundling and unbundling dynamics, and, finally, large-scale exploration properties remains unclear. Recently, indirect experimental evidence suggested that the macroscopic motility of free-swimming bacteria is sensitive to the stochasticity borne by the chemotactic biological circuit [26]. Here, we give direct evidence of this sensitivity.

Conceptually, our analysis starts from the extreme sensitivity of the rotational CCW \rightarrow CW switching to the abundance of the phosphorylated protein CheY-P in the cell. This picture induces a timescale separation, since, at short times, the alternation of CCW and CW rotations keeps a memory of a quasifixed level of CheY-P. This memory is erased at longer times, and we thus expect very different run times and motility features at the macroscopic level.

For the first time, we link the individual motor rotation statistics to the global motility features that we observe in a large number of 3D trajectories of wild-type *E. coli* bacteria. At short observation times, the time persistence of the swimming orientations displays an exponential decay as classically admitted, but with a large distribution of characteristic times within a population of monoclonal bacteria. However, when tracking the cells individually over several tenths of minutes, we identify for each

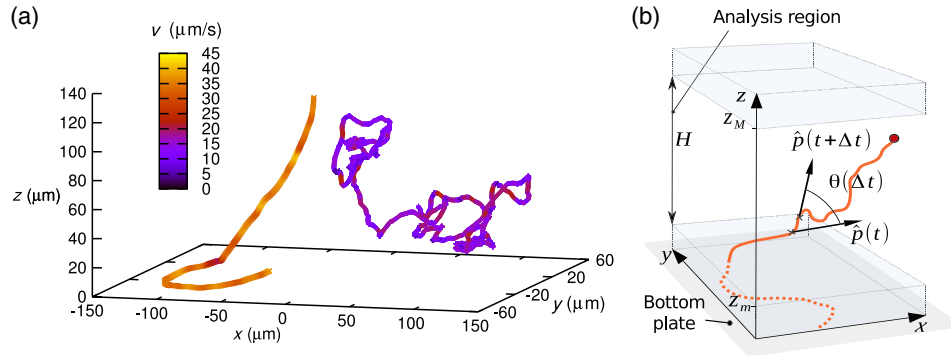
cell a large behavioral variability. The motility data are quantitatively analyzed through a simple model initially proposed by Tu and Grinstein [27] involving the fluctuations of CheY-P triggering the tumbling events. The model is here adapted to render the spatial exploration process. It now explains the occurrence of a large behavioral variability of swimming direction and also why, at short observation times, a large distribution of these is expected over a population. The central outcome of this model is that the persistence time durations naturally follow a log-normal distribution, instead of a standard Poisson distribution. Importantly, we identify a source of measurement bias introduced in most practical situations that is a consequence of such a large distribution of run times. Finally, we discuss the consequences of measuring averaged quantities over a population displaying a large distribution of motility features. This source of measurement bias is relevant in the general framework of experiments on statistical physics of active matter.

II. VARIABILITY OF BACTERIAL MOTILITY IN A POPULATION

To characterize the bacterial motility, we build an automated tracking device suited to follow fluorescent objects and record their 3D trajectories. A swimming bacterium is kept automatically in the center of the visualization field and at the focus of an inverted microscope by a visualization feedback loop acting horizontally on a mechanical stage and vertically on a piezo stage. The method is fully detailed in Ref. [28] by Darnige *et al.* (see also Sec. VI) and was recently used to investigate the swimming of bacteria in a Poiseuille flow [29].

We first monitor more than 100 swimming *E. coli* from different strains (see Sec. VI) in homogeneous diluted suspensions (concentration $\sim 10^5$ bact mL) confined between two horizontal glass slides, 250 μm apart. Figure 1(a) shows two typical trajectories from the same batch of monoclonal wild-type *E. coli*. We center our analysis on pieces of tracks exploring the bulk [Fig. 1(b)], i.e., in a measurement region located 10 μm above the surface and of maximum height $H = 130 \mu\text{m}$. For this series of experiments, the duration of a track is at minimum 8 s. We name these *experiments I*.

The bacterial velocities $\vec{V}(t)$ at each point of the trajectories are obtained by fitting the sequence of coordinates, along X , Y , and Z independently, over segments spanning 0.1 s, using a second-order polynomial. The first derivative of the polynomial evaluated at the center of the segment provides the velocity component. Figure 2 shows an example of a 3D trajectory and its velocity. Typically, the velocity curves for each track are irregular [Fig. 2(b)]. For a single track, the velocity distribution [Fig. 2(c)] shows a peak corresponding to the run phase and a low-velocity tail that might correspond to tumbling events. For the wild-type strain RP437 in a motility buffer, the average of the peak



F1:1 FIG. 1. Lagrangian 3D tracking of bacteria and analysis conditions. (a) RP437 wild-type *E. coli* displaying very different typical
 F1:2 trajectories: persistent trajectory (bact 1: $\tau_p = 12$ s) and nonpersistent trajectory (bact 2: $\tau_p = 0.7$ s). (b) Sketch of the part of the track
 F1:3 used for analysis and angles used for computing $C(\Delta t) = \langle \hat{p}(t) \cdot \hat{p}(t + \Delta t) \rangle = \langle \cos \theta(\Delta t) \rangle$, using a sliding window for an average on
 F1:4 time t .

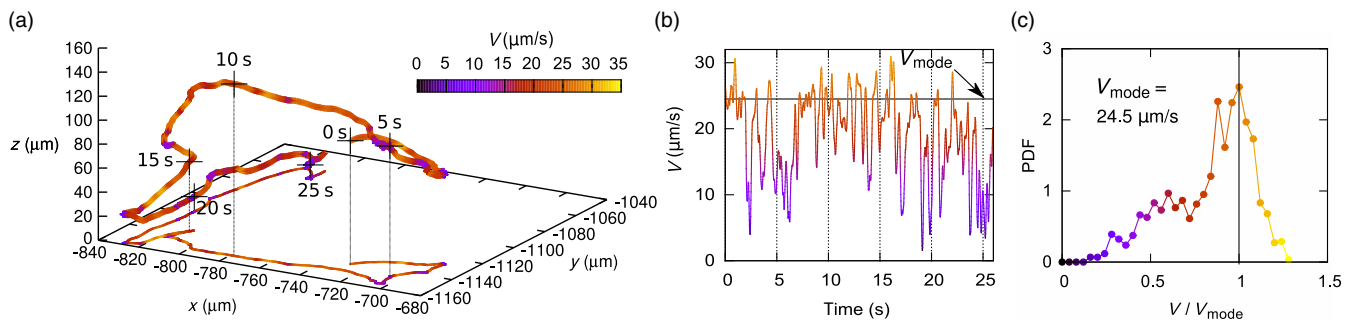
168 values for $V = |\vec{V}(t)|$ over the different tracks is $\langle V \rangle =$
 169 $27 \pm 6 \mu\text{m/s}$.

170 Standard analysis to extract run-time distributions relies
 171 on the identification of tumbling events, usually done by
 172 detecting velocity drops and/or abrupt changes in the
 173 swimming direction [2,6,30]. However, as shown in
 174 Figs. 2(a) and 2(b), abrupt direction changes can take
 175 place without a representative velocity decrease, and
 176 velocity drops are sometimes not associated with reorien-
 177 tation. This observation is consistent with results from
 178 Refs. [30,31]. Moreover, by directly monitoring the flag-
 179 ellar dynamics, Turner *et al.* [31] identify partial flagellar
 180 debundling inducing weak velocity drops and directional
 181 changes. We find that, without a direct observation of the
 182 flagella, run-and-tumble detection requires the choice of
 183 arbitrary criteria. We demonstrate this arbitrariness in the
 184 Appendix A.

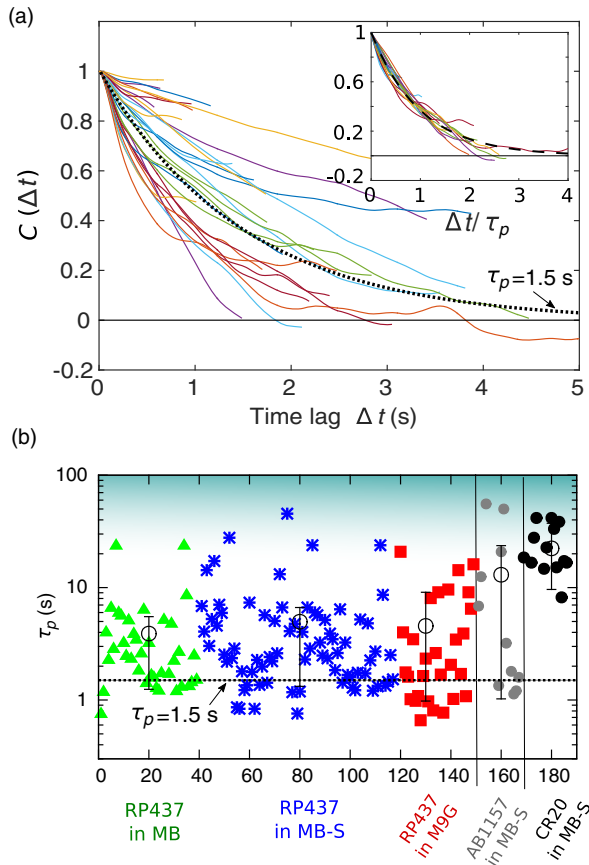
185 Here, in order to characterize the motility features, we do
 186 not seek to explicitly identify the tumbling events. Instead,
 187 we use the orientation correlation function $C(\Delta t)$ as a direct
 188 measurement of the swimming direction persistence. The
 189 director vectors pointing along the track are determined as
 190 $\vec{p} = \vec{V}(t)/V(t)$ for each track. For each trajectory, we
 191 compute $C(\Delta t) = \langle \hat{p}(t) \cdot \hat{p}(t + \Delta t) \rangle = \langle \cos[\theta(\Delta t)] \rangle$, where

192 θ is the angle between swimming directors separated by a
 193 time lag Δt [Fig. 1(b)]. The brackets denote an average over
 194 a time window sliding along the track. To ensure good
 195 statistics, the maximum lag time Δt is chosen as one-tenth
 196 of the total track duration. The orientation correlation
 197 reflects the R&T statistics but advantageously does not
 198 require an *ad hoc* criterion. In Fig. 3(a), 30 orientation
 199 correlation functions obtained from separate tracks of
 200 different bacteria (RP437 wild type in M9G) are displayed as
 201 a function of Δt .

202 From the classical picture of an exponential distribution
 203 of run times, the orientation correlation function is expected
 204 to decay exponentially with a typical decay time of τ_p ,
 205 defining the persistence time of the trajectory. For a
 206 characteristic run time of $\bar{\tau}_{\text{run}} = 1$ s and a distribution of
 207 reorientation angles of mean value $\theta_m = 51^\circ$ [1], one finds
 208 $\tau_p = (\bar{\tau}_{\text{run}}/1 - \langle \cos(\theta) \rangle) = 1.5$ s [32]. Recently, a slight
 209 dependence of this angle on the swimming speed was
 210 demonstrated [33] but is neglected in our study. Taking into
 211 account rotational Brownian diffusion during the run phase
 212 also leads to an exponential decaying correlation function
 213 (see Appendix B). Its contribution represents a slight
 214 modification to τ_p due to the much longer timescales of
 215 Brownian diffusion. The predicted correlation function is



F2:1 FIG. 2. Details of a typical trajectory. (a) 3D trajectory and its projection on the x - y plane, (b) velocity vs time, and (c) velocity
 F2:2 distribution. The marks every 5 s in the 3D track are references for comparison with (b).



F3:1 FIG. 3. Swimming orientation correlations. Experiments I.
 F3:2 (a) Correlation function $C(\Delta t)$ obtained for 30 tracks of different
 F3:3 RP437 bacteria in M9G, showing a large distribution of persistence
 F3:4 times. The correlation functions are fitted with an exponential decay $\exp(-\tau/\tau_p)$ to extract the persistence times τ_p . The
 F3:5 dotted line corresponds to $\tau_p = 1.5$ s as expected from Ref. [1].
 F3:6 Inset: Correlation functions as a function of Δt rescaled by τ_p .
 F3:7 The dashed line is $\exp(-x)$. (b) Persistence times for individual
 F3:8 bacteria of wild-type strains RP437 and AB1157 and smooth
 F3:9 swimmer mutant CR20 in different media (MB, MB-S, and
 F3:10 M9G). Circles and uncertainty bars correspond to the mean and
 F3:11 68% confidence intervals for each group. The blue background
 F3:12 region designates the cutoff from Brownian diffusion. The dotted
 F3:13 line corresponds to the expected $\tau_p = 1.5$ s also represented in
 F3:14 (a). Uncertainty bars indicate the mean and confidence interval
 F3:15 at 68%.
 F3:16

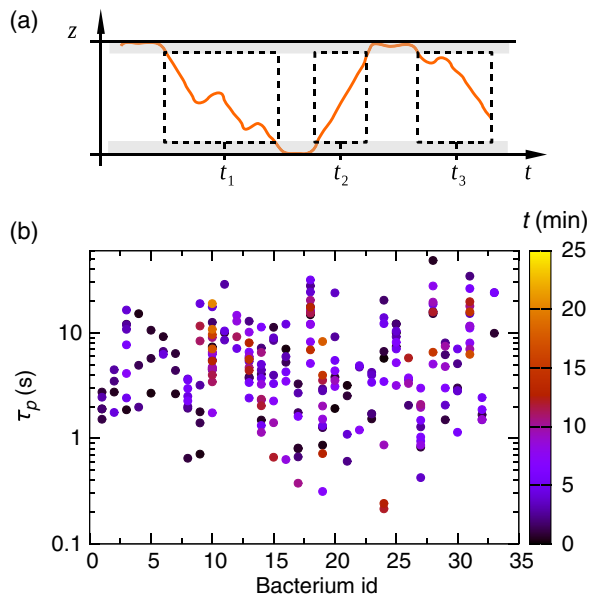
216 represented by the dotted line in Fig. 3(a). Strikingly, the
 217 experimental curves display a broad scattering, indicating a
 218 very large distribution of persistence times within this
 219 monoclonal population of bacteria.

220 By fitting the correlation functions with an exponential
 221 decay $\exp(-\tau/\tau_p)$, we determine the persistence times τ_p
 222 for each track. In Fig. 3(b), we display them on a
 223 logarithmic vertical axis for the strain RP437 in a motility
 224 buffer (MB) and a MB supplemented with serine (MB-S).
 225 In addition, persistence times obtained in a richer medium
 226 (M9G) and for a different wild-type strain AB1157 in

227 MB-S are shown. The results prove that the distribution of
 228 orientation persistence times for wild-type bacteria is very
 229 large. Within statistical errors, they are independent of the
 230 chemical environment (poor or rich), but they could depend
 231 on the strain, being larger in average for the 11 measure-
 232 ments performed on AB1157. For the very persistent
 233 tracks, the observed decorrelation remains weak over the
 234 accessible time lags. The obtained persistence times thus
 235 have a significant uncertainty, but we can be sure that their
 236 decorrelation time will be at least bigger than the time span
 237 of the track ($\tau_p > 8$ s). Finally, we consider the strain
 238 CR20, a smooth swimmer that tumbles only very rarely.
 239 In this case, the time distribution is gathered around the
 240 average $\tau_p = 25 \pm 10$ s, which is close to the Brownian
 241 rotational diffusion constant $\tau_p = \tau_B = 1/2D_r^B$, as expected.
 242 This value is, however, strongly dependent on the bacterial
 243 dimensions and aspect ratio [34,35]. A bacterium modeled
 244 as an ellipsoid of semiaxes $a = 4 \mu\text{m}$ and $b = c = 0.4 \mu\text{m}$
 245 has a persistence time $\tau_p \sim 22$ s, while with $a = 6 \mu\text{m}$ it
 246 has a persistence time 3 times larger, $\tau_p \sim 66$ s [36].
 247 Therefore, the wide distribution of persistence times
 248 for CR20 could arise from the bacterial size distribution.
 249 A possible origin of this dispersion on the measurement
 250 protocol is discussed in Sec. IV C.

251 III. VARIABILITY OF INDIVIDUAL 252 BACTERIAL MOTILITY OVER TIME

253 The large diversity of trajectories here observed over
 254 short times in bacterial populations leads to the question of
 255 its origin. The diversity could arise from a phenotype
 256 multiplicity present in the monoclonal population [37,38],
 257 where each bacterium is characterized by a mean run time;
 258 alternatively, it could be due to temporal variability of the
 259 bacterial behavior, with mean run times varying over the
 260 course of time. To determine which scenario is taking place,
 261 we perform a second series of measurements, *experiments*
 262 *II*, where we follow individual bacteria over very long times
 263 (up to 20 min). In the new configuration, the top and bottom
 264 of the measurement chamber are within the observation
 265 range or the 3D tracker device. We follow individual
 266 bacteria as they alternate between the surfaces and the
 267 bulk, as sketched in Fig. 4(a). For the analysis, individual
 268 tracks are cut in pieces localized entirely in the bulk ($10 \mu\text{m}$
 269 away from the walls). For each piece, we extract the
 270 persistence time from the correlation function. Finally,
 271 for each bacterium, we obtain a list of persistence times
 272 as a function of time. If the population displayed a large
 273 distribution of fixed run-times, one would expect for each
 274 bacterium a sequence of persistence times narrowly dis-
 275 tributed around a characteristic value, but this value would
 276 be different for different bacteria. Figure 4(b) carries a very
 277 different message. For each of the tracks tested, the
 278 persistence times span a range of the same magnitude as



F4:1 FIG. 4. Analysis for long tracks. Experiments II. (a) Sketch
 F4:2 indicating the pieces of track from the same trajectory selected for
 F4:3 demonstrating the behavioral variability. (b) τ_p for pieces of track
 F4:4 from the same trajectories, for 33 different RP437 bacteria in
 F4:5 MB-S. The color represents the starting time of the measurement.
 F4:6 Each bacterium displays a large variation of persistence times.

279 for the whole population using shorter tracking times
 280 (see Fig. 3).

281 Previous studies based on 3D Eulerian tracking tech-
 282 niques [33,39], i.e., on a fixed reference frame, or even the
 283 Lagrangian tracking technique [6] were limited to short
 284 observation times and, consequently, were not able to catch
 285 such slow fluctuations of the run time. The fact that for a
 286 given bacterium the sequence of persistence times is largely
 287 distributed confirms the importance of behavioral variabil-
 288 ity in the motility process. However, due to tracking time
 289 limitations imposed by the bleaching of the fluorescent
 290 signal, we are not able to test precisely to what extent the
 291 behavioral variability contains features which could vary
 292 from one bacterium to the other, stemming from inherent
 293 phenotype variations, as identified, for example, by Dufour
 294 *et al.* [40].

295 IV. MOTILITY AND MOTOR ROTATION 296 STATISTICS

297 The presence of a behavioral variability, as identified
 298 earlier, raises the question of its biochemical origins.
 299 Previous results point toward a definite influence of a
 300 stochastic process in the chemotactic sensory circuit. At the
 301 end of the biochemical cascade, there is a phosphorylation
 302 of a CheY protein (CheY-P) promoting a switch in the
 303 motor rotation from the CCW state (run phase) to the CW
 304 state (tumbling phase). The most accepted picture render-
 305 ing the $\text{CCW} \rightleftharpoons \text{CW}$ transition is a two-state model initially
 306 proposed by Khan and Macnab [41], which considers the

switching of the rotation direction $\text{CCW} \rightarrow \text{CW}$ (equiv- 307
 308 alently, $\text{CW} \rightarrow \text{CCW}$) as an activated process regulated by
 309 the presence of CheY-P. The double-well Gibbs free energy
 310 associated with the transition $\text{CCW} \rightleftharpoons \text{CW}$ depends in a
 311 very sensible way on the CheY-P ($[Y]$) concentration values
 312 near the motor, as shown by Cluzel, Surette, and Leibler
 313 [42]. This strong sensitivity leads naturally to behavioral
 314 variations, as slow fluctuations around the mean value can
 315 change the motility features from preferentially tumbling
 316 (high CheY-P) to preferentially running (low CheY-P). It
 317 also means that at short times the CheY-P level does not
 318 change significantly and motility features remain constant.
 319 Therefore, at a given moment, the motility features should
 320 be largely distributed in a population of bacteria bearing
 321 different CheY-P concentrations. This large distribution
 322 is in essence what is observed in our experiments in
 323 Figs. 3 and 4.

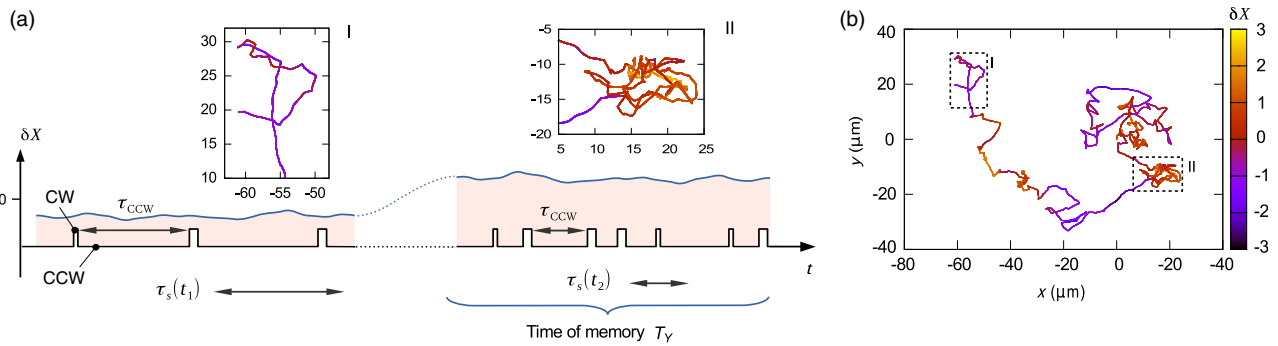
324 A. Quantitative description of the 325 behavioral variability model

326 To rationalize and quantify our experimental findings,
 327 we adapt the simple but enlightening physical model
 328 proposed by Tu and Grinstein [27]. The behavioral vari-
 329 ability (BV) model we present here quantifies the role of
 330 fluctuations of the phosphorylated protein CheY-P in the
 331 regulation of the motor-switching statistics. The key idea is
 332 that the observed typical switching time at a given moment
 333 depends on the instantaneous CheY-P concentration $[Y](t)$.
 334 Then, considering concentration fluctuations around a
 335 mean value ($\delta Y(t) = [Y](t) - [Y_0]$), one obtains a two-state
 336 model with a time-varying barrier describing the $\text{CCW} \rightarrow$
 337 CW switching process. Tu and Grinstein model the δY
 338 fluctuations as an Ornstein-Uhlenbeck process with a
 339 memory (relaxation) time T_Y , hence yielding a Gaussian
 340 distribution for δY values. Note that T_Y is considered to be
 341 larger than typical motor-switching times [see Fig. 5(a)
 342 for the relevant timescales].

343 For small fluctuations of concentration, the average
 344 switching time can be written as

$$\tau_s = \tau_0 e^{-\Delta_n \delta X}. \quad (1)$$

346 Here, δX corresponds to the fluctuations in concentration
 347 normalized by the δY standard deviation σ_Y ; τ_0 is a typical
 348 switching time corresponding to the mean concentration
 349 $[Y_0]$ and $\Delta_n = \alpha(\sigma_Y/Y_0)$. The parameter α is positive [42]
 350 and measures the sensitivity of the switch to variations in
 351 $[Y]$, which means that higher concentrations of CheY-P
 352 lead to shorter run times. Note that, in principle, the two
 353 switching times describing $\text{CCW} \rightarrow \text{CW}$ (run times) or
 354 $\text{CW} \rightarrow \text{CCW}$ (tumbling times) could be modeled with
 355 corresponding parameters τ_0 and Δ_n . However, as the
 356 results from Korobkova *et al.* [21] show that, in contrast
 357 with run times, the distribution of tumble times is expo-
 358 nential, meaning that the equivalent of Δ_n for tumbles is



F5:1 FIG. 5. Heuristic view of the behavioral variability model. (a) Timescales of the tumbling process and the CheY-P concentration
 F5:2 governing them. The switching time τ_s represents the local average of the stochastic run times τ_{CCW} . The switching time τ_s stays
 F5:3 relatively constant during the memory time T_Y and evolves as a function of the normalized CheY-P concentration:
 F5:4 $\delta X = ([Y] - [Y_0]) / \sigma_Y$. (b) 2D projection of the simulated 3D trajectory where the δX fluctuations drive the tumbling process. The
 F5:5 insets correspond to different levels of $[\delta X]$: Inset I depicts a low CheY-P level, and inset II depicts a high CheY-P level.

359 small. Hence, we consider the tumbling times as a
 360 Poissonian process, well described by a single timescale.

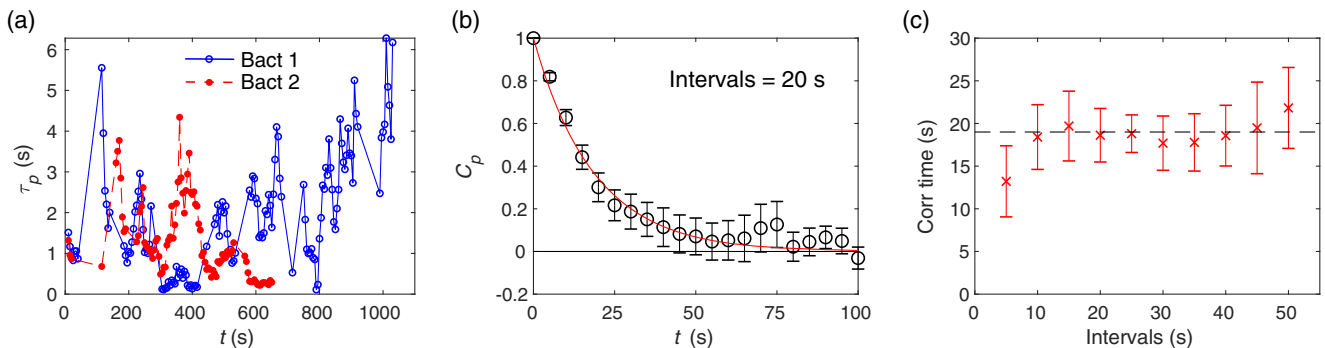
361 Let us first consider the CCW \rightarrow CW switching time
 362 distributions. Each observed time belongs to a Poisson
 363 distribution with a typical time τ_s set by the current CheY-
 364 P concentration $[Y](t)$ [see Eq. (1)]. As a consequence, the
 365 observed switching statistics for an individual bacterium,
 366 when observed over a time interval shorter than the memory
 367 time, should approximately appear as an effective Poisson
 368 process, which is indeed the case, as shown from the collapse
 369 of the rescaled orientation correlation functions onto a single
 370 exponential decay shown in Fig. 3(a). The model provides a
 371 second important outcome. A random choice of a bacterium
 372 in a population is like a random choice of δX , hence defining
 373 a typical switching time τ_s for this bacterium. A Gaussian
 374 distribution for δX , as assumed by the BV model, leads to a
 375 Gaussian distribution of $\ln(\tau_s)$ characterized by an average
 376 $\ln(\tau_0)$ and a standard deviation $\sigma_{\ln \tau_p} = \Delta_n$, yielding natu-
 377 rally a large log-normal distribution of τ_s provided the switch

sensitivity α is large. Note that the power law distribution
 discussed by Tu and Grinstein [27] is obtained in the limit of
 very large Δ_n and not in contradiction with the above
 statement. As τ_s and τ_p are proportional, the distribution
 of $\ln(\tau_p)$ should also be Gaussian.

To illustrate this idea, a very long 3D trajectory is
 synthesized numerically using the switching statistics from
 the BV model. Figure 5(b) shows a 2D projection (see
 Sec. VI for technical details and Sec. IV C for the parameter
 values). The simulated trajectory contains very persistent
 (inset I) and very nonpersistent (inset II) parts. The colors
 represent the local values of δX illustrating the direct
 influence of the slow variations of CheY-P concentration
 on the bacterial motility, hence explaining the observed
 behavioral variability.

B. Memory time

The evolution of persistence times τ_p along individual
 trajectories displays large variations. It is shown in Fig. 6(a)



F6:1 FIG. 6. Determination of the memory time from experiments II. (a) Persistence times τ_p computed over pieces of span 20 s and shifted
 F6:2 5 s for two different bacteria. Gaps larger than 5 s between consecutive points correspond to lapses in which the bacteria are swimming
 F6:3 close to surfaces. (b) Persistence times self-correlation function C_p using pieces of 20 s. Points represent the average over the ensemble
 F6:4 of bacteria. (c) Correlation time of the persistence times as a function of the lengths of the pieces. We extract the memory time to be
 F6:5 $T_Y = 19.0 \pm 1.3$ s.

396 for the case of two different bacteria continuously tracked
 397 for 11 and 17 min. The values of τ_p for each track are
 398 extracted from intervals of span 20 s shifted 5 s along the
 399 trajectory. Gaps larger than 5 s between consecutive points
 400 correspond to lapses in which the bacterium is swimming
 401 close to a surface. Analyzing, for example, the bacterium of
 402 the blue longer trajectory, at time 300 s (5 min) it displays a
 403 persistence time close to 0.1 s, in contrast with a persistence
 404 time close to 5 s around time 1000 s (~ 17 min). This
 405 temporal variation of τ_p is considered in the framework of
 406 the BV model. The memory time T_Y is then a central
 407 parameter of the BV model, as it provides a natural
 408 separation between short-time measurements and long-time
 409 measurements. Therefore, for a correct statistical interpretation
 410 of the results, τ_p values must be extracted from
 411 pieces of tracks not longer than the memory time T_Y .

412 We estimate the memory time T_Y from the long-time
 413 tracking data in experiments II, using the following procedure.
 414 For each bacterial trajectory, we compute a sequence
 415 of τ_p using intervals of a specific duration. For each sequence
 416 of τ_p , we compute the self-correlation function of persistence
 417 times, $C_p(t) = \langle \ln \tau_p(t+t') \ln \tau_p(t') \rangle - \langle \ln \tau_p \rangle^2$, where
 418 the average is done over t' . The average of C_p over the ensemble
 419 of trajectories is fitted with an exponential, giving the
 420 correlation time [Fig. 6(b)]. With this procedure, we
 421 investigate different lengths of intervals [Fig. 6(c)], finding
 422 that the correlation times grow with the duration of the
 423 interval until saturation at the value of the memory time
 424 $T_Y \approx 19.0 \pm 1.3$ s.

425 C. Comparison with the model

426 The BV model depends on several parameters: the
 427 memory time T_Y , the mean switch time and sensitivity
 428 τ_0 and Δ_n , respectively, the rotational diffusion coefficient
 429 D_r^B , and the dimensionless rotational diffusion coefficient
 430 \tilde{D}_r^{eff} used to model the reorientation during tumble (see
 431 Sec. VI for details). We determine T_Y from the experiments,
 432 while the rest of the parameters are fitted using the
 433 following protocol. A long simulated trajectory is generated
 434 and cut in pieces of duration 20 s, similar to the
 435 analysis of the experimental tracks, and the persistence time
 436 is computed for each piece. We look for the values of the
 437 parameters that best agree with the experimental values of
 438 the first four moments of the distribution of $\ln \tau_p$. The result
 439 is $\tau_0 = 1.53$ s, $\Delta_n = 1.62$, $D_r^B = 0.025$ s $^{-1}$, and $\tilde{D}_r^{\text{eff}} = 3.86$.
 440 Note that the velocity does not appear in the fit, because we
 441 compare simulations and experiments using the persistence
 442 times, which depend only on the orientations.

443 Figure 7(a) compares the experimental distribution of
 444 $\ln \tau_p$ with the results from simulations using the optimal
 445 parameters. The agreement is very good, with two features
 446 that need discussion. First, in agreement with the BV
 447 model, the distributions are not exactly Gaussian but

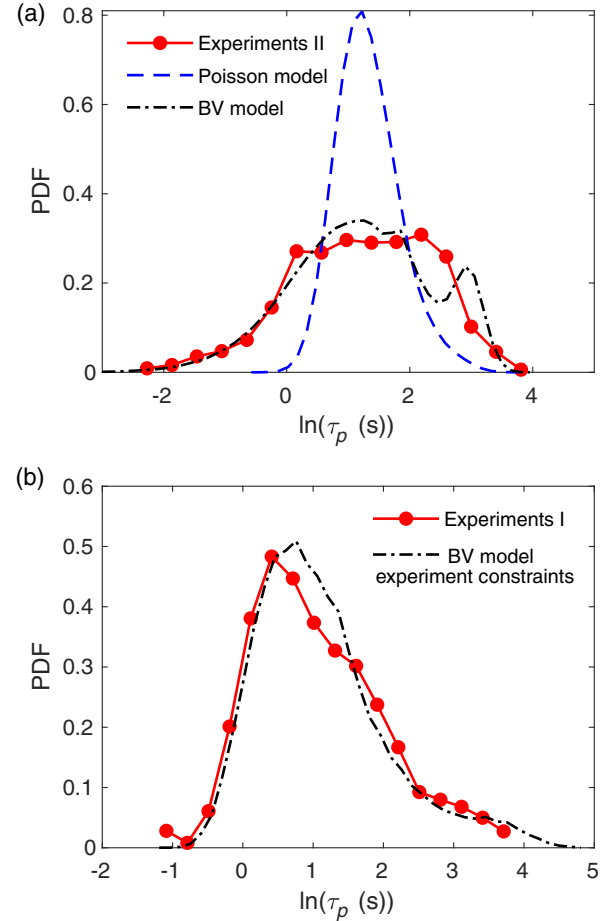


FIG. 7. Probability density function of the logarithm of persistence times ($\ln \tau_p$). (a) The values τ_p are extracted from pieces of track from experiments II that last 20 s. Simulations using two different models are shown: The Poisson model does not reproduce the experiments, while the BV model reproduces the main features. (b) The experimental distribution corresponds to the combined RP437 bacteria in all media, from Fig. 3 in experiments I. “BV model experiment constraints” are determined from the same simulations of “BV model” but analyzing pieces of trajectories that follow the experimental constraints in this case. It reproduces experiments I without additional free parameters.

448 present a negative excess kurtosis. With 63% probability,
 449 the switch times are in the range $[\tau_0 e^{-\Delta_n}, \tau_0 e^{\Delta_n}] =$
 450 $[0.30$ s, 7.7 s]. Hence, there is no complete separation of
 451 timescale with T_Y . As a consequence, in each piece, δX is not
 452 constant, and the measured and simulation distributions
 453 result from the mixture of different values of τ_s . Note that
 454 shorter pieces would imply too few tumble events and would
 455 make it unreliable to use the orientation correlation function.
 456 A perfect log-normal distribution could be observed if there
 457 was a good separation of timescales, allowing a choice of
 458 intervals such that $\tau_0 \ll T_{\text{interval}} \ll T_Y$.

459 The second feature is the small peak at $\ln \tau_p \approx 3$ in the
 460 simulations. This peak corresponds to pieces of the

461 trajectory where no single tumble took place. The change in
 462 orientation is due only to rotational diffusion during a run.
 463 Because $\tau_B = 1/2D_r^B \approx 20$ s is similar to T_Y , no complete
 464 reorientation occurs in the interval, resulting in a distribu-
 465 tion of τ_p for nontumbling swimmers. In fact, the persist-
 466 ence times for the nontumbling bacteria [strain CR20 from
 467 experiments I, Fig. 3(b)] coincide with this peak. This
 468 feature should also be present in experiments, but, as
 469 discussed in Sec. II, D_r^B depends strongly on the bacterial
 470 dimensions, which vary within the population. This
 471 dispersion of rotational diffusion and other imperfections
 472 blur this peak in the experiments, contrary to the simu-
 473 lations, where all swimmers are identical. Note that, despite
 474 of the diversity, the fitted value of D_r^B matches closely the
 475 prediction made in Sec. II for ellipsoidal swimmers.

476 Since the pieces of trajectories are of a finite length, the
 477 orientation correlation function is not perfectly sampled,
 478 and, even for a constant switch time τ_s , the persistence
 479 times τ_p obtained from an exponential fit would present
 480 some dispersion. To test whether the observed dispersion is
 481 due only to the data analysis protocol, we perform
 482 simulations with a Poisson model. For this test, we look
 483 for the best parameters to reproduce the first fourth
 484 moments of the distribution of $\ln \tau_p$, setting $\Delta_n = 0$. The
 485 result is $\tau_0 = 1.18$ s, $D_r^B = 0.026$ s⁻¹, and $\tilde{D}_r^{\text{eff}} = 1.61$.
 486 Figure 7(a) presents the resulting distribution, which is far
 487 from the experimental one. We conclude that a Poisson
 488 process cannot explain the broad distribution of persistence
 489 times observed experimentally.

490 Finally, for consistency, we return to the persistence
 491 times obtained in Fig. 3 from experiments I. In this
 492 experimental protocol, the trajectories are selected within
 493 a certain height (10–140 μm from the surface) and longer
 494 than 8 s. The corresponding experimental distribution of
 495 $\ln(\tau_p)$ for RP437 bacteria in all media [Fig. 7(b)] displays a
 496 clear positive skewness, which differs strikingly from the
 497 experimental measures of Fig. 7(a), done using the same
 498 bacterial strain and confinement and a similar chemical
 499 environment. This difference originates from a measure-
 500 ment bias built into the analysis of Fig. 7(b) (and Fig. 3).
 501 The bias is a consequence of a preferential selection of long
 502 trajectories staying essentially in the x - y plane, with limited
 503 bounds in the vertical direction. The skewness is enhanced
 504 by the broad distribution of run times, since very persistent
 505 swimmers will likely quit the measurement region in a very
 506 short time, hence privileging small persistence times. The
 507 curve “BV model” represents the distribution of persistence
 508 times from simulations of the BV model that fit the
 509 experiments in Fig. 7(a) (experiments I). When this same
 510 simulation is analyzed by taking pieces following strictly
 511 the experimental constraints, on both duration and vertical
 512 spatial exploration, the resulting distribution (“BV model
 513 experiment constraints”) compares very well and notice-
 514 ably without any additional fitting parameter, to the
 515 experimental curve in Fig. 7(b) (experiments II).

V. CONCLUSIONS

516 We have shown that the 3D spatial exploration of an
 517 adapted *E. coli* reflects a behavioral variability that we
 518 associate with intrinsic noise in the chemotaxis pathway
 519 controlling the run-and-tumble sequence. Our results for
 520 free-swimming bacteria are consistent with models describ-
 521 ing motor-switching dynamics based on tethered cell
 522 measurements. We identified a large log-normal distribu-
 523 tion of persistent times stemming from the slow fluctua-
 524 tions of an internal variable accounting for the CheY-P
 525 concentration near the motors. In the context of many
 526 recent works on statistical physics of active matter, we
 527 suggest that this large variability should be included in the
 528 description of bacterial fluids. This variability is expected
 529 to influence the computation of averaged quantities like
 530 diffusivity, viscosity, or any constitutive relations of macro-
 531 scopic transport processes.

532 The broad distribution of run times is likely to introduce
 533 measurement biases in practical situations. Here, we reduce
 534 the bias by taking pieces of trajectories of equal length, not
 535 larger than the memory time. Mixing trajectories of different
 536 lengths can result in highly distorted distributions.

537 The large distribution of motility features has been related
 538 to the time bacteria spend close to surfaces. As an example,
 539 the existence of a large distribution of motor-switching
 540 statistics was found crucial to understand large-scale
 541 upstream bacterial contamination of narrow channels [26],
 542 where substantial transport occurs along surfaces [43–46].

543 We expect the chemotactic drift to be sensitive to the
 544 distribution of CheY-P concentrations, since a nonlocal
 545 spatiotemporal coupling will take place between chemical
 546 gradients and bacterial concentration. This sensitivity
 547 should be taken into account in future motility modeling.
 548 Finally, these findings may also impact quantitative mod-
 549 eling on how bacterial populations react to environmental
 550 changes, colonize space, swarm in a biofilm [47], or
 551 interact with other communities.

VI. MATERIALS AND METHODS

A. Bacterial strains and culture

554 We use the wild-type strains RP437 and AB1157 and a
 555 smooth swimmer mutant strain CR20 (ΔCheY) expressing
 556 yellow fluorescent protein (YFP) from a plasmid. Bacteria
 557 are grown overnight at 30 °C in M9G medium [M9 minimal
 558 medium supplemented with glucose (4 g/L), casamino
 559 acids (1 g/L), MgSO₄ (2 mM), and CaCl₂ (0.1 mM)] plus
 560 the corresponding antibiotics, up to optical density = 0.5 at
 561 595 nm. Cells are then washed 3 times by centrifugation at
 562 2000 g for 5 min and suspended in a motility buffer (10 mM
 563 potassium phosphate buffer $p\text{H} \sim 7.0$, 0.1 mM EDTA,
 564 1 μM L-methionine, and 10 mM sodium L-lactate), sup-
 565 plemented with polyvinylpyrrolidone (PVP-360 kDa
 566 0.002%) and, when indicated, with L-Serine (0.04 g/mL).
 567

568

B. The 3D Lagrangian tracker

569 We develop a device for keeping individual microscopic
570 objects—as swimming bacteria—in focus, as they move in
571 microfluidic chambers [28]. The system is based on real-
572 time image processing, determining the displacement of the
573 stage to keep the chosen object at a fixed position in the
574 observation frame. The z displacement of the stage is based
575 on the refocusing of the fluorescent object that keeps the
576 moving object in focus. The algorithm for z determination
577 is designed for not being affected by photobleaching.

578 The instrument is mounted on an epifluorescent inverted
579 microscope (Zeiss-Observer, Z1) with a high magnification
580 objective (100 × /0.9 DIC Zeiss EC Epiplan-Neofluar), an
581 x - y mechanically controllable stage with a z piezomover
582 from Applied Scientific Instrumentation (ms-2000-flat-top-
583 xyz), and a digital camera ANDOR iXon 897 EMCCD.
584 The device works nominally at 30 frames per second on a
585 512 × 512 pix² matrix, but a faster tracking speed of 80 Hz
586 can be achieved by reducing the spatial resolution to
587 128 × 128 pix². It provides images of the object and its
588 track coordinates with respect to the microfluidic device.

589 The tracking limitations come essentially from the z
590 exploration range, restricted by the working distance of
591 150 μm of the objective. In the x - y plane, the spatial
592 limitations are virtually nonexistent, since the stage dis-
593 placement can be as long as 15 cm, which is much bigger
594 than the typical sizes of the sample (a few millimeters).
595 Details of the apparatus are given in Ref. [28], as well as an
596 exhaustive explanation of a method for correcting the
597 mechanical backlash typically affecting these systems and
598 a discussion of the device’s performance and limitations.

C. Experimental geometries and bacteria tracking

600 We monitor hundreds of single *E. coli* in a drop of a diluted
601 homogeneous suspension (concentration $\sim 10^5$ bact/mL)
602 squeezed between two horizontal glass slides. The drop
603 has typically a diameter of 1 mm. The gap between the two
604 glass plates is 250 μm. For experiments I, displayed in
605 Fig. 3, only pieces of 3D trajectories remaining between the
606 vertical bounds $z_m = 10$ μm from the bottom surface and
607 $z_M = 140$ μm, the highest possible height, and lasting more
608 than 8 s are taken into account. For the set of very long tracks
609 in Fig. 4, experiments II, the gap between the glass plates is
610 also 250 μm, but the whole trajectories are captured, as they
611 alternate between the bottom and top. For the analysis, only
612 pieces farther than 10 μm from the surfaces are taken into
613 account.

614 The velocities are determined from second-order
615 Savitzky-Golay filtering of the coordinates over 0.1 s,
616 resulting in uncertainties close to 5% [36]. For each track,
617 the velocity distribution shows a peak corresponding to the
618 mean run velocity and a low-velocity tail corresponding to
619 the contribution of sudden velocity drops (Fig. 2). Peak

620 velocities are on average $\langle V \rangle = 27 \pm 6$ μm/s. To compute
621 the correlation function $C(\Delta t)$, the average is made over
622 time, and the lag time is offset by 0.2 s to avoid the short-
623 time decorrelation due to wobbling [36,48]. The correlation
624 function is then normalized by its value at 0.2 s to yield 1 at
625 the lag time origin.

D. Track simulations using the BV model

626 Swimmers are described by their position \vec{r} , orientation
627 \hat{p} , and the instantaneous value of the normalized fluctua-
628 tions of the CheY-P concentration $\delta X = ([Y] - [Y_0])/\sigma_Y$.
629 During the run phase, they obey the equations
630

$$\dot{\vec{r}} = V\hat{p}, \quad (2)$$

$$\dot{\hat{p}} = \sqrt{D_r^B}(I - \hat{p}\hat{p})\vec{\eta}(t), \quad (3) \quad 631$$

$$\delta\dot{X} = -\delta X/T_Y + \sqrt{2/T_Y}\xi(t), \quad (4) \quad 633$$

634 where V is the swim velocity, D_r^B is the rotational diffusion
635 coefficient, T_Y is the memory time, $(I - \hat{p}\hat{p})$ is a projector
636 orthogonal to \hat{p} , ξ is a white noise of zero mean and
637 correlation $\langle \xi(t)\xi(s) \rangle = \delta(t-s)$, and $\vec{\eta}$ is a white noise
638 vector of zero mean, where the components have correla-
639 tions $\langle \eta_i(t)\eta_k(s) \rangle = \delta_{ik}\delta(t-s)$.
640

641 The BV model yields a relation between the character-
642 istic switching time for the transition CCW → CW (run to
643 tumble) and the CheY-P concentration. As a simplification,
644 we assume that, due to the small cellular dimensions, all six
645 flagella operate at the same CheY-P concentration and that
646 the reverse of the rotation direction of a single flagellum is
647 enough to trigger a tumble. Hence, the probability to
648 tumble in Δt would be $6\Delta t/\tau_s$. To simplify notation, we
649 absorb the factor 6 into τ_0 , resulting in a tumble proba-
650 bility $\Delta t e^{\Delta_n \delta X} / \tau_0$.
651

652 The BV model predicts that the characteristic switching
653 time for the transition CCW → CW (tumble to run) is also
654 given from an activated process. But, as the corresponding
655 value of Δ_n is small, the tumble duration is given by a
656 Poisson process with characteristic time τ_1 . In addition, the
657 reorientation dynamics during a tumble needs to be
658 modeled. *A priori*, the link between motor switch and
659 tumble is far from being trivial, as, in principle, one needs
660 to account for the hydrodynamically complex bundling and
661 unbinding process of the multiflagellated *E. coli* bacteria
662 [49,50]. Here, we rather follow a simple effective approach
663 inspired by Saragosti, Silberzan, and Buguin [51]. We
664 model the reorientation dynamics during tumbling as an
665 effective rotational diffusion process with a coefficient D_r^{eff} .
666 Defining the dimensionless combination $\tilde{D}_r^{\text{eff}} = D_r^{\text{eff}}\tau_1$, the
667 dimensionless tumble durations are sorted from an expo-
668 nential distribution with a typical time equal to one, and,
669 during a tumble, the dynamics is
670

$$\dot{\vec{r}} = 0, \tag{5}$$

$$\dot{\hat{p}} = \sqrt{\tilde{D}_r^{\text{eff}}} (I - \hat{p} \hat{p}) \vec{\eta}(t), \tag{6}$$

$$\delta \dot{X} = 0. \tag{7}$$

After the tumble phase, a new run phase starts.

ACKNOWLEDGMENTS

The authors thank Dr. Reinaldo García García for useful discussions, Professor Axel Bugin for bacterial strains, and Professor Igor Aranson for comments on the manuscript. This work was supported by the ANR grant ‘‘BacFlow’’ ANR-15-CE30-0013 and the Franco-Chilean Ecosud Collaborative Program C16E03. N.F.-M. thanks the Pierre-Gilles de Gennes Foundation for financial support. A. L. and N.F.-M. acknowledge support from the ERC Consolidator Grant PaDyFlow under Grant Agreement No. 682367. R.S. acknowledges the Fondecyt Grant No. 1180791 and Millennium Nucleus Physics of Active Matter of the Millennium Scientific Initiative of the Ministry of Economy, Development and Tourism (Chile). V.A.M. was funded by ERC AdG 340877 (PHYSAPS) and Joliot-Curie Chair from ESPCI. E. C. and R. S. thank the support from Laboratoire International Associé ‘‘Matière: Structure et dynamique’’ (LIA-MSD), CNRS-France. This work has received the support of Institut Pierre-Gilles de Gennes (Équipement d’Excellence, ‘‘Investissements d’avenir,’’ Program No. ANR-10-EQPX-34).

APPENDIX A: RUN DURATION ANALYSIS

Figure 8 displays a series of analyses on a single trajectory, evidencing that tumble detection is criterium dependent. Here, we set a threshold velocity, cutoff V , and identify as runs all the continuous parts of the track where the bacterial velocity is above the prescribed threshold. The plot demonstrates that, by changing the cutoff value for the velocity, we can obtain average run times of duration 1–8 s.

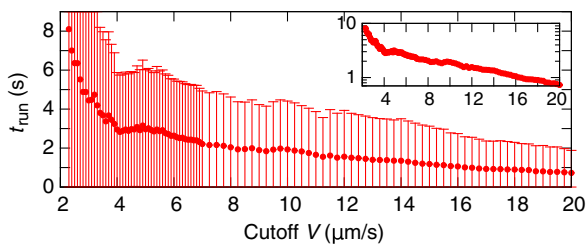


FIG. 8. Average run duration as a function of the threshold in bacterial velocity (cutoff V). The runs are identified as continuous parts of the track where $V > \text{cutoff } V$. The plot demonstrates that an arbitrary choice of velocity drops along the trajectory leads to arbitrary run-time duration. Inset: Log-normal plot.

APPENDIX B: PERSISTENCE CORRELATION FUNCTION

The orientation correlation function is defined as

$$C(\tau) = \langle \hat{p}(t) \cdot \hat{p}(t + \tau) \rangle = \langle \cos[\theta(\tau)] \rangle, \tag{B1}$$

where \hat{p} is the director vector and the average is done over time t .

To compute the correlation function, we use a kinetic theory approach. The object under study is the distribution function $f(\hat{p}, t)$, which gives the probability that a bacterium has an orientation \hat{p} at time t . In this context, the correlation function is obtained assuming that the initial condition at $t = 0$ is with the bacterium pointing in a specific direction, say, \hat{p}_0 . Hence, we have to compute $C(\tau) = \langle \hat{p}(\tau) \cdot \hat{p}_0 \rangle$, where now the average is over the distribution function. At the end, another average, over \hat{p}_0 , should be done. In practice, this last average is unnecessary by the isotropy of space, because the first average gives already a value independent of \hat{p}_0 .

The distribution function obeys the kinetic equation [52,53]

$$\frac{\partial f}{\partial t} = -Lf, \tag{B2}$$

with

$$f(\hat{p}, 0) = \delta(\hat{p} - \hat{p}_0) \tag{B3}$$

and L the evolution operator. Two models must be considered. In the case of Brownian rotational diffusivity,

$$Lf = -D_r^B \nabla_{\hat{p}}^2 f, \tag{B4}$$

where D_r^B is the rotational diffusion coefficient and $\nabla_{\hat{p}}^2$ is the angular part of the Laplacian. In the case of tumbling with a characteristic switch time τ_s ,

$$Lf = \frac{1}{\tau_s} \left[f - \int d\hat{p}' W(\hat{p}', \hat{p}) f(\hat{p}') \right]. \tag{B5}$$

The kernel $W(\hat{p}', \hat{p})$ gives the probability that for a swimmer with director \hat{p}' , after tumbling, the new director is \hat{p} . It is normalized to $\int d\hat{p} W(\hat{p}', \hat{p}) = 1$, indicating that some director \hat{p} must be chosen. If the space is isotropic, the kernel depends only on the relative angle between the directors, that is, $W(\hat{p}', \hat{p}) = w(\hat{p}' \cdot \hat{p})$. Finally, if tumbling and diffusion are present, the operator is just the sum of both.

If the space is isotropic, the evolution operator is also isotropic, which in this case implies that it commutes with the angular Laplacian $\nabla_{\hat{p}}^2$. Therefore, both operators share eigenfunctions, which are the spherical harmonics $Y_{lm}(\hat{p})$. Then, there are eigenvalues λ_l ,

$$LY_{lm} = \lambda_l Y_{lm}, \quad (\text{B6})$$

750 that, by isotropy, do not depend on the second index m . For
751 the diffusion case, the eigenvalues are known exactly, while
752 for tumbling they are proportional to $1/\tau_s$ and depend on
753 the kernel model. In summary,

$$\lambda_l = D_r^B l(l+1) + 1/(a_l \tau_s), \quad (\text{B7})$$

754 where a_l are dimensionless parameters of the order of 1 that
755 depend on the kernel w .

756 Using the basis of the spherical harmonics, the solution
757 of the kinetic equation (B2) is
758

$$f(\hat{p}, t) = \sum_{lm} f_{lm}(0) Y_{lm}(\hat{p}) e^{-\lambda_l t}, \quad (\text{B8})$$

760 where $f_{lm}(0)$ depend on the initial condition (B3).

761 Now, the correlation function is

$$C(t) = \langle \hat{p}(t) \cdot \hat{p}_0 \rangle \quad (\text{B9})$$

$$= \int d\hat{p} \hat{p}_0 \cdot \hat{p} f(\hat{p}, t) \quad (\text{B10})$$

$$= \sum_{lm} f_{lm}(0) e^{-\lambda_l t} \hat{p}_0 \cdot \int d\hat{p} \hat{p} Y_{lm}(\hat{p}). \quad (\text{B11})$$

766 Using that \hat{p} can be written as a linear combination of Y_{1m} ,
767 with $m = 0, \pm 1$ and the orthogonality of the spherical
768 harmonics, it is obtained that the integral is not vanishing
769 only for $l = 1$. Combining factors, one obtains
770

$$C(t) = C_0 e^{-t/\tau_p}, \quad (\text{B12})$$

771 where

$$\tau_p = \frac{a_1 \tau_s}{1 + a_1 \tau_s / \tau_B} \quad (\text{B13})$$

773 and $\tau_B = 1/(2D_r^B)$ is the Brownian decorrelation time.

774 In the classical picture, where all bacteria have a single
775 value for τ_s , the decorrelation time τ_p is single valued also.
776 When τ_s is broadly distributed, the decorrelation time τ_p
777 also follows a broad distribution for $\tau_p \ll \tau_B$, and it is
778 bounded from above by τ_B . Finally, in the description of
779 Berg and Brown [1], the tumble angles are distributed with
780 a peak at 63° . In this case, $a_1 = 1/(1 - \langle \cos \theta \rangle)$ [51].
781

783
784 [1] H. C. Berg and D. A. Brown, *Chemotaxis in Escherichia*
785 *coli Analysed by Three-Dimensional Tracking*, *Nature*
786 (London) **239**, 500 (1972).

787 [2] H. C. Berg, *E. coli in Motion* (Springer, New York, 2004).

- [3] J. Saragosti, V. Calvez, N. Bournaveas, B. Perthame, A. Buguin, and P. Silberzan, *Directional Persistence of Chemotactic Bacteria in a Traveling Concentration Wave*, *Proc. Natl. Acad. Sci. U.S.A.* **108**, 16235 (2011). 788-791
- [4] U. Alon, L. Camarena, M. G. Surette, B. A. y Arcas, Y. Liu, S. Leibler, and J. B. Stock, *Response Regulator Output in Bacterial Chemotaxis*, *EMBO J.* **17**, 4238 (1998). 792-794
- [5] H. C. Berg, *Random Walks in Biology* (Princeton University, Princeton, NJ, 1993). 795-796
- [6] Z. Qu, F. Z. Temel, R. Henderikx, and K. S. Breuer, *Changes in the Flagellar Bundling Time Account for Variations in Swimming Behavior of Flagellated Bacteria in Viscous Media*, *Proc. Natl. Acad. Sci. U.S.A.* **115**, 1707 (2018). 797-801
- [7] X.-L. Wu and A. Libchaber, *Particle Diffusion in a Quasi-Two-Dimensional Bacterial Bath*, *Phys. Rev. Lett.* **84**, 3017 (2000). 802-804
- [8] D. Saintillan and M. J. Shelley, *Active Suspensions and Their Nonlinear Models*, *C.R. Phys.* **14**, 497 (2013). 805-806
- [9] M. C. Marchetti, J. F. Joanny, S. Ramaswamy, T. B. Liverpool, J. Prost, M. Rao, and R. A. Simha, *Hydrodynamics of Soft Active Matter*, *Rev. Mod. Phys.* **85**, 1143 (2013). 807-809
- [10] A. P. Solon, Y. Fily, A. Baskaran, M. E. Cates, Y. Kafri, M. Kardar, and J. Tailleur, *Pressure Is Not a State Function for Generic Active Fluids*, *Nat. Phys.* **11**, 673 (2015). 810-812
- [11] J. Schwarz-Linek, J. Arlt, A. Jepsen, A. Dawson, T. Vissers, D. Miroli, T. Pilizota, V. A. Martinez, and W. C. K. Poon, *Escherichia coli as a Model Active Colloid: A Practical Introduction*, *Colloids Surf. B* **137**, 2 (2016). 813-816
- [12] P. Galajda, J. Keymer, P. Chaikin, and R. Austin, *A Wall of Funnels Concentrates Swimming Bacteria*, *J. Bacteriol.* **189**, 8704 (2007). 817-819
- [13] C. Dombrowski, L. Cisneros, S. Chatkaew, R. E. Goldstein, and J. O. Kessler, *Self-Concentration and Large-Scale Coherence in Bacterial Dynamics*, *Phys. Rev. Lett.* **93**, 098103 (2004). 820-823
- [14] A. Sokolov and I. S. Aranson, *Reduction of Viscosity in Suspension of Swimming Bacteria*, *Phys. Rev. Lett.* **103**, 148101 (2009). 824-826
- [15] J. Gachelin, G. Miño, H. Berthet, A. Lindner, A. Rousselet, and E. Clément, *Non-Newtonian Viscosity of Escherichia coli Suspensions*, *Phys. Rev. Lett.* **110**, 268103 (2013). 827-829
- [16] H. M. López, J. Gachelin, C. Douarache, H. Auradou, and E. Clément, *Turning Bacteria Suspensions into Superfluids*, *Phys. Rev. Lett.* **115**, 028301 (2015). 830-832
- [17] A. Sokolov, M. M. Apodaca, B. A. Grzybowski, and I. S. Aranson, *Swimming Bacteria Power Microscopic Gears*, *Proc. Natl. Acad. Sci. U.S.A.* **107**, 969 (2010). 833-835
- [18] R. Di Leonardo, L. Angelani, D. DellArciprete, G. Ruocco, V. Iebba, S. Schippa, M. P. Conte, F. Mecarini, F. De Angelis, and E. Di Fabrizio, *Bacterial Ratchet Motors*, *Proc. Natl. Acad. Sci. U.S.A.* **107**, 9541 (2010). 836-839
- [19] H. Wioand, F. G. Woodhouse, J. Dunkel, J. O. Kessler, and R. E. Goldstein, *Confinement Stabilizes a Bacterial Suspension into a Spiral Vortex*, *Phys. Rev. Lett.* **110**, 268102 (2013). 840-843
- [20] A. Kaiser, A. Peshkov, A. Sokolov, B. ten Hagen, H. Löwen, and I. S. Aranson, *Transport Powered by Bacterial Turbulence*, *Phys. Rev. Lett.* **112**, 158101 (2014). 844-847

- 848 [21] E. Korobkova, T. Emonet, J. M. G. Vilar, T. S. Shimizu, and
849 P. Cluzel, *From Molecular Noise to Behavioural Variability*
850 *in a Single Bacterium*, *Nature (London)* **428**, 574 (2004).
851 [22] E. A. Korobkova, T. Emonet, H. Park, and P. Cluzel, *Hidden*
852 *Stochastic Nature of a Single Bacterial Motor*, *Phys. Rev.*
853 *Lett.* **96**, 058105 (2006).
854 [23] T. Emonet and P. Cluzel, *Relationship between Cellular*
855 *Response and Behavioral Variability in Bacterial Chemo-*
856 *taxis*, *Proc. Natl. Acad. Sci. U.S.A.* **105**, 3304 (2008).
857 [24] T. L. Min, P. J. Mears, L. M. Chubiz, C. V. Rao, I. Golding,
858 and Y. R. Chemla, *High-Resolution, Long-Term Charac-*
859 *terization of Bacterial Motility Using Optical Tweezers*,
860 *Nat. Methods* **6**, 831 (2009).
861 [25] F. Wang, H. Shi, R. He, R. Wang, R. Zhang, and J. Yuan,
862 *Non-equilibrium Effect in the Allosteric Regulation of the*
863 *Bacterial Flagellar Switch*, *Nat. Phys.* **13**, 710 (2017).
864 [26] N. Figueroa-Morales, A. Rivera, R. Soto, A. Lindner, E.
865 Altshuler, and E. Clément, *E. coli “Super-Contaminates”*
866 *Narrow Ducts Fostered by Broad Run-Time Distribution*,
867 *Sci. Adv.* **6**, eaay0155 (2020), [https://advances.sciencemag](https://advances.sciencemag.org/content/6/11/eaay0155)
868 [.org/content/6/11/eaay0155](https://advances.sciencemag.org/content/6/11/eaay0155).
869 [27] Y. Tu and G. Grinstein, *How White Noise Generates Power-*
870 *Law Switching in Bacterial Flagellar Motors*, *Phys. Rev.*
871 *Lett.* **94**, 208101 (2005).
872 [28] T. Darnige, N. Figueroa-Morales, P. Bohec, A. Lindner, and
873 E. Clément, *Lagrangian 3D Tracking of Fluorescent Micro-*
874 *scopic Objects in Motion*, *Rev. Sci. Instrum.* **88**, 055106
875 (2017).
876 [29] G. Junot, N. Figueroa-Morales, T. Darnige, A. Lindner, R.
877 Soto, H. Auradou, and E. Clément, *Swimming Bacteria in*
878 *Poiseuille Flow: The Quest for Active Bretherton-Jeffery*
879 *Trajectories*, *Europhys. Lett.* **126**, 44003 (2019).
880 [30] M. Molaie, M. Barry, R. Stocker, and J. Sheng, *Failed*
881 *Escape: Solid Surfaces Prevent Tumbling of Escherichia*
882 *coli*, *Phys. Rev. Lett.* **113**, 068103 (2014).
883 [31] L. Turner, L. Ping, M. Neubauer, and H. C. Berg, *Visual-*
884 *izing Flagella while Tracking Bacteria*, *Biophys. J.* **111**,
885 630 (2016).
886 [32] P. S. Lovely and F. W. Dahlquist, *Statistical Measures of*
887 *Bacterial Motility and Chemotaxis*, *J. Theor. Biol.* **50**, 477
888 (1975).
889 [33] K. M. Taute, S. Gude, S. J. Tans, and T. S. Shimizu, *High-*
890 *Throughput 3D Tracking of Bacteria on a Standard Phase*
891 *Contrast Microscope*, *Nat. Commun.* **6**, 8776 (2015).
892 [34] F. Perrin, *Mouvement Brownien d’un Ellipsoïde (I).*
893 *Dispersion Diélectrique pour des Molécules Ellipsoïdales*,
894 *J. Phys. Radium* **5**, 497 (1934).
895 [35] F. Perrin, *Mouvement Brownien d’un Ellipsoïde (II). Rota-*
896 *tion Libre et Dépolarisation des Fluorescences. Translation*
897 *et Diffusion de Molécules Ellipsoïdales*, *J. Phys. Radium* **7**,
898 1 (1936).
899 [36] N. Figueroa-Morales, *Active Bacterial Suspensions: From*
900 *Microhydrodynamics to Transport Properties in Micro-*
901 *fluidic Channels*, Ph. D. thesis, UPMC, Paris, 2016.
902 [37] W. K. Smits, O. P. Kuipers, and J.-W. Veening, *Phenotypic*
903 *Variation in Bacteria: The Role of Feedback Regulation*,
904 *Nat. Rev. Microbiol.* **4**, 259 (2006).
[38] A. J. Waite, N. W. Frankel, and T. Emonet, *Behavioral*
905 *Variability and Phenotypic Diversity in Bacterial Chemo-*
906 *taxis*, *Annu. Rev. Biophys.* **47**, 595 (2018), pMID
907 29618219. 908
[39] M. Wu, J. W. Roberts, S. Kim, D. L. Koch, and M. P.
909 DeLisa, *Collective Bacterial Dynamics Revealed Using a*
910 *Three-Dimensional Population-Scale Defocused Particle*
911 *Tracking Technique*, *Appl. Environ. Microbiol.* **72**, 4987
912 (2006). 913
[40] S. Y. S. Dufour, S. Gillet, S. Frankel, D. B. Weibel, and T.
914 Emonet, *Direct Correlation between Motile Behavior and*
915 *Protein Abundance in Single Cells*, *PLoS Comput. Biol.* **12**,
916 e1005041 (2016). 917
[41] S. Khan and R. M. Macnab, *The Steady-State Counter-*
918 *clockwise/Clockwise Ratio of Bacterial Flagellar Motors Is*
919 *Regulated by Protonmotive Force*, *J. Mol. Biol.* **138**, 563
920 (1980). 921
[42] P. Cluzel, M. Surette, and S. Leibler, *An Ultrasensitive*
922 *Bacterial Motor Revealed by Monitoring Signaling Proteins*
923 *in Single Cells*, *Science* **287**, 1652 (2000). 924
[43] E. Altshuler, G. Miño, C. Pérez-Penichet, L. del Río, A.
925 Lindner, A. Rousselet, and E. Clément, *Flow-Controlled*
926 *Densification and Anomalous Dispersion of E. coli through*
927 *a Constriction*, *Soft Matter* **9**, 1864 (2013). 928
[44] N. Figueroa-Morales, E. Altshuler, A. Hernández-García, A.
929 Lage-Castellanos, and E. Clément, *Two-Dimensional Con-*
930 *tinuous Model for Bacterial Flows through Microfluidic*
931 *Channels*, *Rev. Cubana Fis.* **30**, 3 (2013). 932
[45] N. Figueroa-Morales, G. L. Miño, A. Rivera, R. Caballero,
933 E. Clément, E. Altshuler, and A. Lindner, *Living on the*
934 *Edge: Transfer and Traffic of E. coli in a Confined Flow*,
935 *Soft Matter* **11**, 6284 (2015). 936
[46] A. J. T. M. Mathijssen, N. Figueroa-Morales, G. Junot, É.
937 Clément, A. Lindner, and A. Zöttl, *Oscillatory Surface*
938 *Rheotaxis of Swimming E. coli Bacteria*, *Nat. Commun.* **10**,
939 3434 (2019). 940
[47] G. Ariel, A. Rabani, S. Benisty, J. D. Partridge, R. M.
941 Harshey, and A. Be’er, *Swarming Bacteria Migrate by*
942 *Lévy Walk*, *Nat. Commun.* **6**, 8396 (2015). 943
[48] S. Bianchi, F. Saglimbeni, and R. Di Leonardo, *Holo-*
944 *graphic Imaging Reveals the Mechanism of Wall*
945 *Entrapment in Swimming Bacteria*, *Phys. Rev. X* **7**,
946 011010 (2017). 947
[49] N. C. Darnton, L. Turner, S. Rojevsky, and H. C. Berg, *On*
948 *Torque and Tumbling in Swimming Escherichia coli*,
949 *J. Bacteriol.* **189**, 1756 (2007). 950
[50] P. J. Mears, S. Koirala, C. V. Rao, I. Golding, and Y. R.
951 Chemla, *Escherichia coli Swimming Is Robust against*
952 *Variations in Flagellar Number*, *eLife* **3**, e01916 (2014). 953
[51] J. Saragosti, P. Silberzan, and A. Buguin, *Modeling E. coli*
954 *Tumbles by Rotational Diffusion. Implications for Chemo-*
955 *taxis*, *PLoS One* **7**, e35412 (2012). 956
[52] D. Saintillan, *The Dilute Rheology of Swimming Suspen-*
957 *sions: A Simple Kinetic Model*, *Exp. Mech.* **50**, 1275
958 (2010). 959
[53] R. Soto, *Kinetic Theory and Transport Phenomena* (Oxford
960 University, New York, 2016), Vol. 25. 961
962